The Company of Biologists

RESEARCH ARTICLE

Underwater flight by the planktonic sea butterfly

David W. Murphy[1],[*],[‡], Deepak Adhikari[1], Donald R. Webster[1] and Jeannette Yen[2]

ABSTRACT

In a remarkable example of convergent evolution, we show that the zooplanktonic sea butterfly *Limacina helicina* 'flies' underwater in the same way that very small insects fly in the air. Both sea butterflies and flying insects stroke their wings in a characteristic figure-of-eight pattern to produce lift, and both generate extra lift by peeling their wings apart at the beginning of the power stroke (the well-known Weis-Fogh 'clap-and-fling' mechanism). It is highly surprising to find a zooplankter 'mimicking' insect flight as almost all zooplankton swim in this intermediate Reynolds number range (*Re*=10–100) by using their appendages as paddles rather than wings. The sea butterfly is also unique in that it accomplishes its insect-like figure-of-eight wing stroke by extreme rotation of its body (what we call 'hyper-pitching'), a paradigm that has implications for micro aerial vehicle (MAV) design. No other animal, to our knowledge, pitches to this extent under normal locomotion.

KEY WORDS: Pteropods, Zooplankton, Swimming, Weis-Fogh mechanism, Insect flight, Convergent evolution

INTRODUCTION

Zooplankton swim to find food and mates and to escape from and avoid predators. Indeed, in what is likely the largest animal migration on Earth in terms of biomass, many zooplankton species swim hundreds of meters to the water surface every night to graze and avoid predation (Hays, 2003). How these millimeter-to-centimeter scale organisms efficiently propel themselves at intermediate Reynolds numbers is thus of great interest. Zooplankton and small insects swim and fly, respectively, in an intermediate Reynolds number regime ($Re=ul/\nu$ =10–1000, where u is the characteristic velocity scale, l is the characteristic length scale and ν is kinematic viscosity) in which both viscous and inertial forces are important. However, they generally use different locomotion techniques. Most zooplankton species (e.g. copepods and euphausiids) in this *Re* regime paddle through the water with drag-based propulsion in which viscous drag on a hairy, jointed appendage is maximized during the power stroke and minimized on the recovery stroke (Strickler, 1975; Yen, 2000; Kiørboe et al., 2014). In contrast, insects such as fruit flies use their wings as airfoils to generate aerodynamic lift (and drag) on both power and recovery strokes (Dickinson et al., 1999). Insects may generate additional lift via unsteady aerodynamic interactions between the wings such as the well-known Weis-Fogh 'clap-and-fling' mechanism (Weis-Fogh, 1973; Lighthill, 1973; Ellington, 1984a,b; Dickinson et al., 1999).

The Weis-Fogh mechanism, including variants such as the 'partial clap-and-fling', 'near clap-and-fling' and 'clap-and-peel', is used by a wide variety of flying insect species (Ellington, 1984a). The technique was first noted in the tiny wasp *Encarsia formosa* (Weis-Fogh, 1973), which hovers by beating its sub-millimeter-length wings at a frequency of approximately 400 Hz. Use of the Weis-Fogh mechanism appears to be an obligate behavior for small insects flying at less than about *Re*=100, including thrips (Ellington, 1984a; Santhanakrishnan et al., 2014), the greenhouse white-fly *Trialeurodes vaoparium* (Weis-Fogh, 1975) and the parasitoid wasp species *Muscidifurax raptor* and *Nasonia vitripennis* (Miller and Peskin, 2009). For the slightly larger *Drosophila* species, flying at *Re*>100, the Weis-Fogh mechanism is rarely used in free flight but is seen when the animal is tethered (Vogel, 1967; Lehmann et al., 2005). Larger flying insects, such as moths and butterflies (Ellington, 1984a) and locusts in climbing flight (Cooter and Baker, 1977), have also been observed using the Weis-Fogh mechanism. Experimental measurements of the flow generated by the Weis-Fogh mechanism in freely flying insects have proven prohibitive because of the small time and length scales involved, though studies of tethered insects (Dickinson and Götz, 1996; Fuchiwaki et al., 2013) and dynamically scaled models (Dickinson et al., 1999; Lehmann et al., 2005; Lehmann and Pick, 2007) have offered valuable insight. Computational modeling has also proven helpful for understanding the fluid dynamics of flight by tiny flying insects (Miller and Peskin, 2005, 2009; Santhanakrishnan et al., 2014; Jones et al., 2015).

It has been suggested, based on kinematics measurements, that marine mollusks such as *Clione limacina* (Satterlie et al., 1985; Szymik and Satterlie, 2011), *Clione antarctica* (Borrell et al., 2005) and *Limacina helicina* (Chang and Yen, 2012) also perform a version of the clap-and-fling at a similar intermediate *Re*. These marine organisms potentially offer the opportunity to experimentally measure flows induced by a freely 'flying' animal using the Weis-Fogh mechanism because of the larger sizes of these mollusks and their lower appendage beat frequencies (compared with tiny flying insects). Furthermore, the appendage kinematics and body pitching of these larger organisms beating at lower frequencies could be resolved with much greater detail. *Limacina helicina* locomotion was investigated in the current study.

The zooplankter *L. helicina* is a pelagic thecosomatous sea snail known as the sea butterfly. *Limacina helicina* is ecologically important for the large biomass it maintains in polar pelagic ecosystems. Furthermore, because its shell sinks when the animal dies, *L. helicina* is geochemically important as a major conduit of carbon to the deep ocean (Bednaršek et al., 2012). In temperate regions, *L. helicina* reaches shell diameters of 1–4 mm and swims at speeds of 10–50 mm s^{-1}, whereas in the sub-Arctic, their shells may grow to 14 mm, with swimming speeds reaching 120 mm s^{-1} (Chang and Yen, 2012). In contrast to many other zooplankton, pelagic pteropods such as *L. helicina* (see Figs 1 and 2; Movies 1 and 2) possess smooth, wing-like swimming appendages (parapodia) that flap in a complex three-dimensional stroke

[1]School of Civil and Environmental Engineering, Georgia Institute of Technology, Atlanta, GA 30332-0355, USA. [2]School of Biology, Georgia Institute of Technology, Atlanta, GA 30332-0230, USA.
*Present address: Department of Mechanical Engineering, The Johns Hopkins University, Baltimore, MD 21218-2681, USA.

‡Author for correspondence (dwmurphy@jhu.edu)

Journal of Experimental Biology

List of symbols and abbreviations

l	length scale
MAV	micro aerial vehicle
PIV	particle image velocimetry
Re	Reynolds number
Re_c	chordwise Reynolds number
t'	time normalized by stroke period
u	velocity scale
xyz	global coordinate systems
$x'y'z'$	body-centered coordinate systems
α	angle between wings
θ	body angle
ν	kinematic viscosity

pattern resembling the wingbeat kinematics of flying insects (Chang and Yen, 2012). Indeed, the chordwise Reynolds number (Re_c) of *L. helicina* swimming (Re_c=40–90) lies between the Re_c of flight by thrips (Re_c=5–35) (Weis-Fogh, 1973; Santhanakrishnan et al., 2014) and fruit flies (Re_c=100–300) (Dickinson et al., 1999). These similarities suggest that, like insect flight, pteropod swimming also may be lift based and raise the possibility that pteropods may have converged to the same lift generation mechanisms used by many insects (e.g. the Weis-Fogh clap-and-fling). This convergence would have occurred along a completely different evolutionary lineage as Insecta and Gastropoda are thought to have diverged 550 million years ago (Valentine, 1997; McGhee, 2011). Lift-based flapping locomotion is well known among larger aquatic animals, such as sea turtles, but would be highly unusual for aquatic animals on the scale of zooplankton (at low Re), where the ratio of lift-to-drag on a flapping appendage decreases dramatically. The potential benefit to pteropods, however, is that flapping appendages are more mechanically efficient than rowing appendages at all swimming speeds (Walker and Westneat, 2000). In addition, flapping strokes generate greater vertical force at the Reynolds numbers characteristic of pteropod swimming (Jones et al., 2015). Efficient generation of lift is particularly important to *L. helicina* as it possesses a dense aragonite shell which causes it to rapidly sink when not swimming or suspended from its parachute-like mucus feeding web (Gilmer and Harbison, 1986; Bednaršek et al., 2012; Chang and Yen, 2012).

Our hypothesis is that, despite living in a low Re aquatic environment, this pteropod employs lift-based locomotion techniques similar to those used by many small, flying insects. In order to determine whether pteropod swimming is employing lift- or drag-based propulsion, we filmed free-swimming individuals of *L. helicina* in the laboratory to obtain highly resolved three-
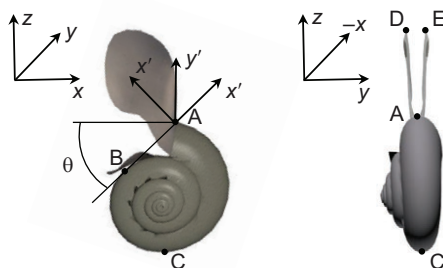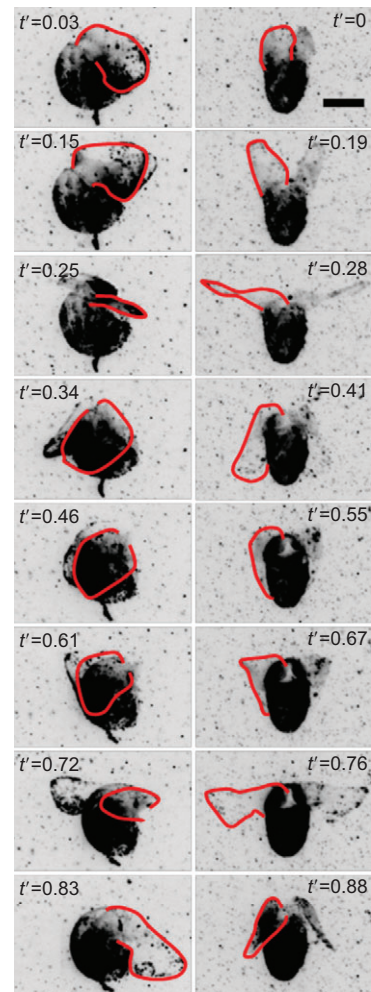

Fig. 2. Pteropod wing stroke. Sequence of inverted-color particle image velocimetry (PIV) images for pteropod 1 (left) and pteropod 3 (right) illustrating the stroke cycle. t' is time normalized by the stroke period. The scale bar represents 1 mm. One wing in each image is outlined in red.

dimensional flow fields surrounding the pteropod. We measured three-dimensional kinematics of the pteropod body and wingtips from the same recordings. This is the first study to measure detailed kinematics and the flow fields created by a freely 'flying' organism using the Weis-Fogh mechanism and provides the most complete picture to date of how the clap-and-fling is used in free 'flight'.

MATERIALS AND METHODS

Limacina helicina (Phipps 1774) were collected off the coast near the Hadfield Marine Station in Newport, OR, USA, in June 2011 and were shipped overnight to Atlanta, GA, USA, where they were kept in buckets of artificial seawater at 32 ppt in an environmental chamber set at 12°C. Tomographic particle image velocimetry (PIV) measurements of freely swimming animals were collected at 500 frames s^{-1} within 1 week using the four-camera system described by Murphy et al. (2012, 2013). The flow was seeded with 11.7 μm mean diameter hollow glass spheres and illumination was provided by near-infrared lasers (808 nm). The pteropods generally swam vertically upwards until they reached the water surface, at which point they sank to the bottom and began swimming upwards again. Three recordings in which an animal entered the illuminated 16×10.5×8.5 mm measurement volume were suitable for processing and further analysis (designated as pteropods 1, 2 and 3).

Fig. 1. Pteropod morphology and coordinate systems. Schematic diagram of a pteropod showing the global (xyz) and body-centered ($x'y'z'$) coordinate systems, the locations of the tracked points (A–E) and definition of the body angle θ.
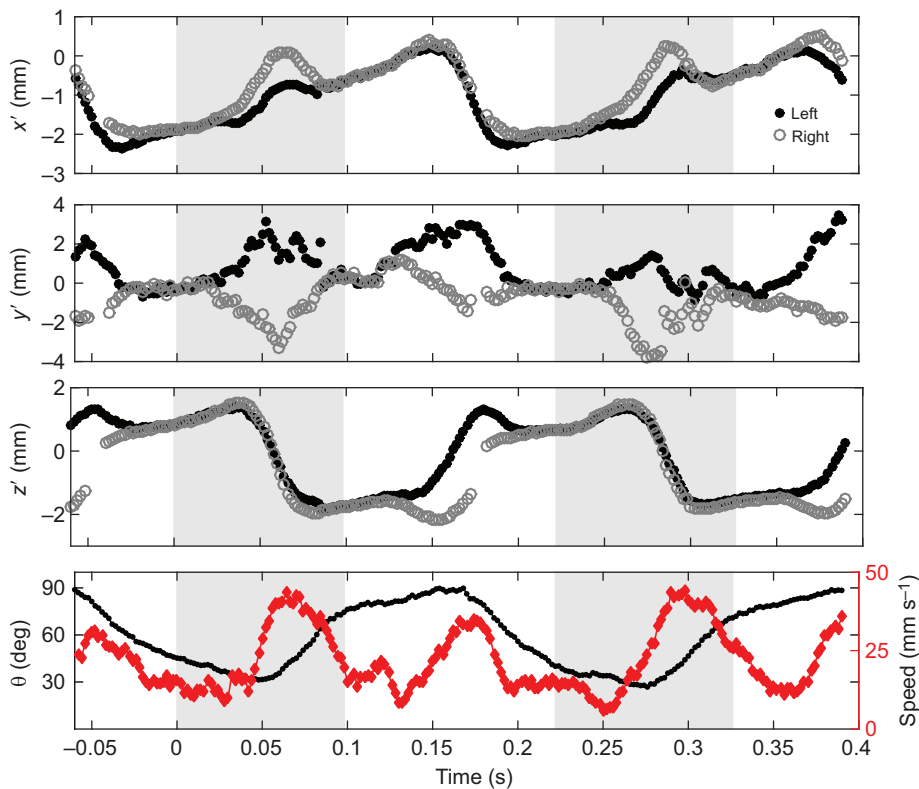
Fig. 3. Pteropod wingtip and body kinematics. Kinematics of left and right wingtips, body angle θ (black) and animal speed (red) for pteropod 1 over slightly more than two complete strokes. The power stroke period is shaded gray. Wingtip positions are given in the body-centered coordinate system.

LaVision's DaVis 8.2 software was used for processing. A preliminary mapping function for all four cameras was determined from images of a calibration plate. A self-calibration procedure reduced disparity errors and hence corrected the calibration mapping function for all cameras. Particle intensity volumes were then reconstructed in the volume using the MLOS-SMART algorithm. A visual hull method was applied on the reconstructed volume to remove reconstruction artifacts caused by the presence of the organism and consequently avoid contaminating local fluid velocity vectors during cross-correlation (Adhikari and Longmire, 2012). Cross-correlating masked volume pairs separated by 2 ms yielded fluid velocity fields. The interrogation volume was $64 \times 64 \times 64$ voxels. Using a 75% overlap resulted in fields of $64 \times 42 \times 34$ vectors with a vector spacing of 0.25 mm.

Table 1 shows morphological and kinematic characteristics of the three pteropods, as well as the Re_c for each individual. The four videos synchronously collected for tomographic PIV analysis were also used to extract kinematics of the pteropods in three dimensions. For each animal, three locations on the shell (labeled A, B and C in Fig. 1) and the two wingtips (labeled D and E) were manually tracked in DLTdv5 software (Hedrick, 2008). The sagittal planes of pteropods 1 and 2 were closely aligned with the imaging planes of

the cameras. This alignment allowed calculation of each pteropod's body angle θ (Fig. 1). In addition, points A, B and C were used to calculate each pteropod's geometric center assuming a circular shell, thereby allowing calculation of the trajectories in the x–z plane for pteropods 1 and 2. Wingtips (points D and E) were tracked for pteropod 1, but could not be tracked for pteropod 2 because of its smaller size and highly transparent parapodia. For pteropod 1, wingtip coordinates in the body-centered coordinate system were calculated by translating and rotating the coordinates relative to the origin located at point A (Fig. 1). The sagittal plane of pteropod 3 was aligned perpendicular to the imaging planes of the cameras; the body angle and geometric center trajectory could not be extracted in this case. However, the alignment of pteropod 3 allowed hydrodynamic analysis of the flow around and between the parapodia. The wing opening angle α, formed by points D, A and E in Fig. 1, was also calculated for pteropod 3.

RESULTS
Wingtip kinematics

We provide the following overview of the *L. helicina* stroke (Figs 2 and 3; see Movies 1 and 2). We first note that the parapodia are highly flexible and may both twist along their span and bend along

Table 1. Measured morphological and swimming characteristics of the three recorded pteropods

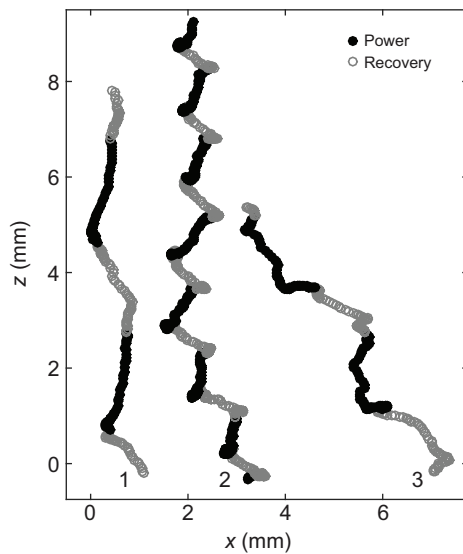| Pteropod	Shell diameter (mm)	Wing length (mm)	Mid-wing chord (mm)	Wing aspect ratio	Mean power stroke period (ms)	Mean recovery stroke period (ms)	Mean stroke period (ms)	Mean swimming speed (mm s^{-1})	Re_c
1	1.92±0.03	2.86±0.27	0.55	5.2	98±6	120	214	22.1±11.7	60
2	1.60±0.07	2.14±0.22	0.50	4.3	101±8	127±4	228±6	14.9±9.1	49
3	2.03±0.01	2.19±0.01	0.56	3.9	120	113±5	230	26.2±18.2	53

Re_c, chordwise Reynolds number.

Fig. 4. Pteropod swimming trajectories. Upward swimming trajectories of pteropods 1–3. Points indicate the geometric center of the shell for pteropods 1 and 2 and the average of shell points B and C for pteropod 3.

their chord throughout the complex stroke (Chang and Yen, 2012). The pteropod begins its power stroke with its wings raised together above its shell. The tips of the arching wings touch but are separated at the wing base, forming a canopy. The wingtips roll along each other and separate from the leading edge to the trailing edge, twisting along their span as they begin the power stroke. The wings stroke diagonally downwards, ending the power stroke by lying across the shell. The wingtips extend beyond the shell and bend in the spanwise direction to approach or touch each other. Much of this spanwise bending, which occurs at the extreme positions (i.e. the
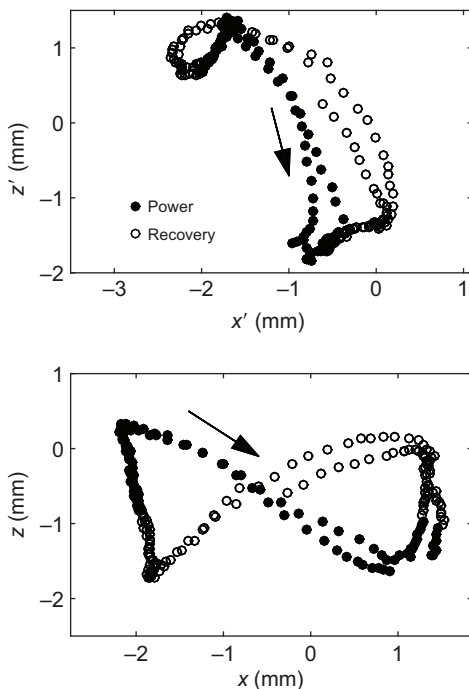

Fig. 5. Transformation of pteropod wingtip coordinates by hyper-pitching. Sagittal view of wingtip coordinates for pteropod 1 in body-centered (top) and global (bottom) coordinate systems.
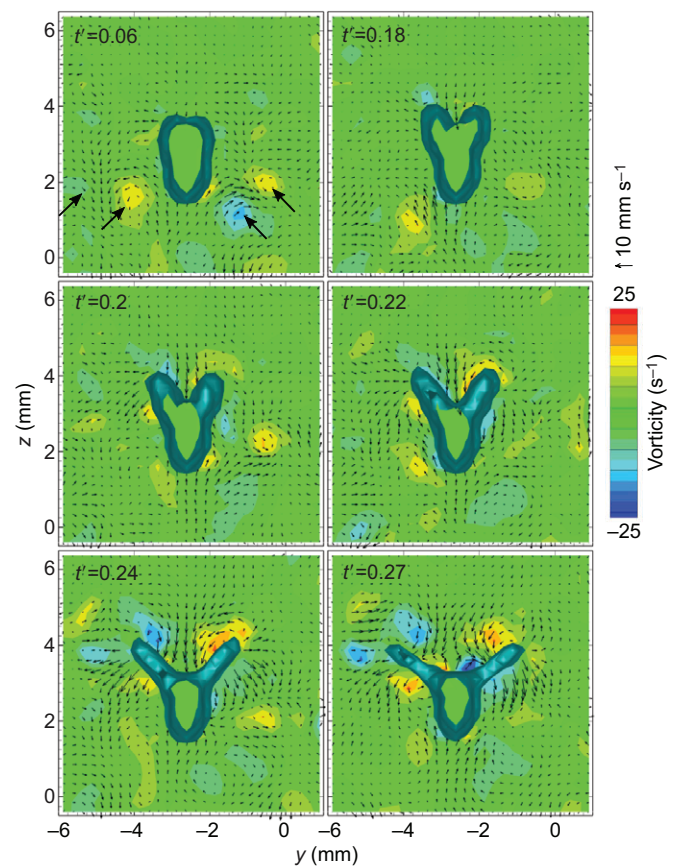

Fig. 6. Flow measurements of Weis-Fogh 'near-fling' maneuver by the pteropod. Sequence of flow measurements in a plane bisecting a *Limacina helicina* specimen that is performing a Weis-Fogh near-fling. Color contours represent the *x*-component of vorticity. Vectors, which lie tangent in the plane, indicate flow direction and magnitude. Pairs of oppositely signed vortices on either side of the animal (marked with black arrows at $t'=0.06$) result from the previous stroke.

beginning and end of the power stroke), appears to occur in the narrow, proximal half of the wing; the broad, distal wingtips appear relatively flat throughout the stroke. The power stroke induces a 50–60 deg rotation of the pteropod about its transverse axis and a rapid increase in its speed to approximately 40 mm s^{-1}. In preparation for the recovery stroke, the pteropod then slides its wings upwards along its body as its speed decreases to about 10 mm s^{-1}. In the recovery stroke, the pteropod strokes its wings diagonally downwards in the opposite direction, again increasing the animal's speed (to about 35 mm s^{-1}) and pitching the pteropod in the opposite direction. Finally, the pteropod recovers its wings to their original position above the shell. The pteropod gains elevation during both power and recovery strokes, resulting in an upward sawtooth trajectory (see Fig. 4) as it beats it wings at a frequency of 5–9 Hz (Chang and Yen, 2012).

After accounting for the extreme rotation of *L. helicina*, its wing kinematics show striking similarity to those of insects flying in the same *Re* regime. In a body-centered coordinate system, the wingtip traces a complex trajectory (Fig. 5) in which it is not clear how useful lift could be generated. In a 'global' coordinate system (i.e. one that translates with the animal but does not rotate) that thereby includes the effect of body pitching, the pteropod effectively strokes its parapodia in a figure-of-eight pattern (Fig. 5). Figure-of-eight wingtip trajectories are common in flying insects (Ellington, 1984a) and, when combined with a large angle of attack in both power and
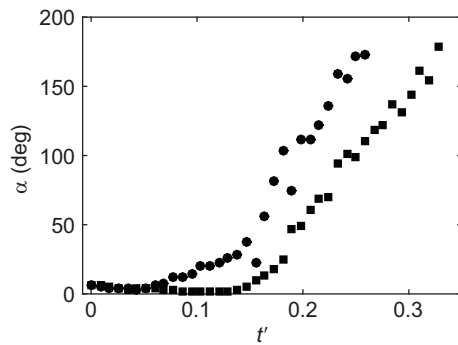
Fig. 7. Angle between wings over time. Time variation of wing opening angle α during the fling phase of two consecutive power strokes of pteropod 3. The squares correspond to the stroke shown in Fig. 2.

recovery strokes, have been shown to produce the most lift when compared with other, insect-inspired wingtip trajectories (Lehmann and Pick, 2007). *Limacina helicina* uses a large angle of attack (46 deg in the power stroke and 49 deg in the recovery stroke), a technique that allows it to maximize lift. Furthermore, its stroke planes for both power and recovery strokes lie approximately 29 deg above the horizontal plane. Drag on its appendages, acting parallel to the stroke plane, therefore provides additional upward vertical force during both power and recovery strokes; this technique is also used by many insects (Wang, 2004).
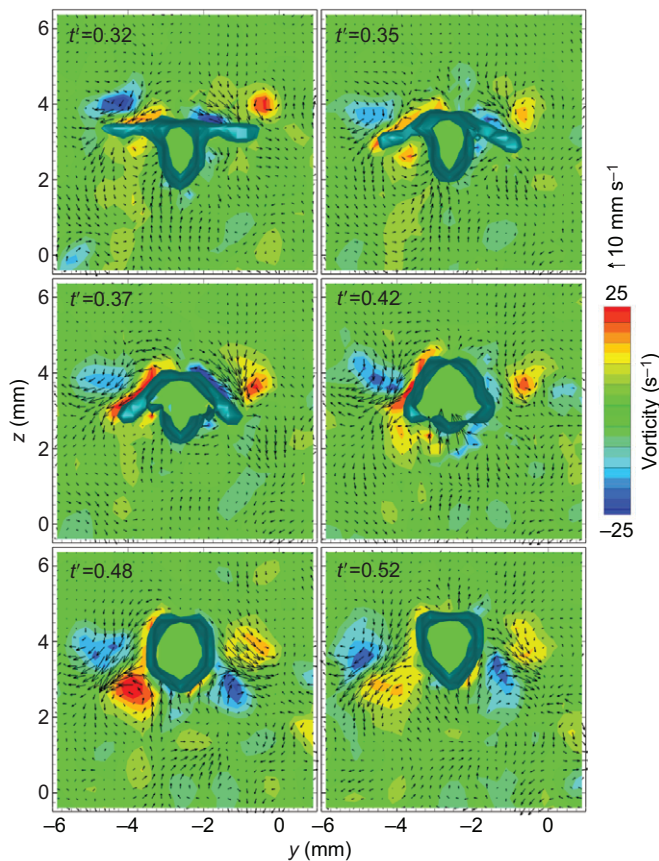

Fig. 8. Flow fields during the end of the power stroke. Color contours represent the *x*-component of vorticity. Vectors, which lie tangent in the plane, indicate flow direction and magnitude. The transverse plane shown is the same as in Fig. 6.
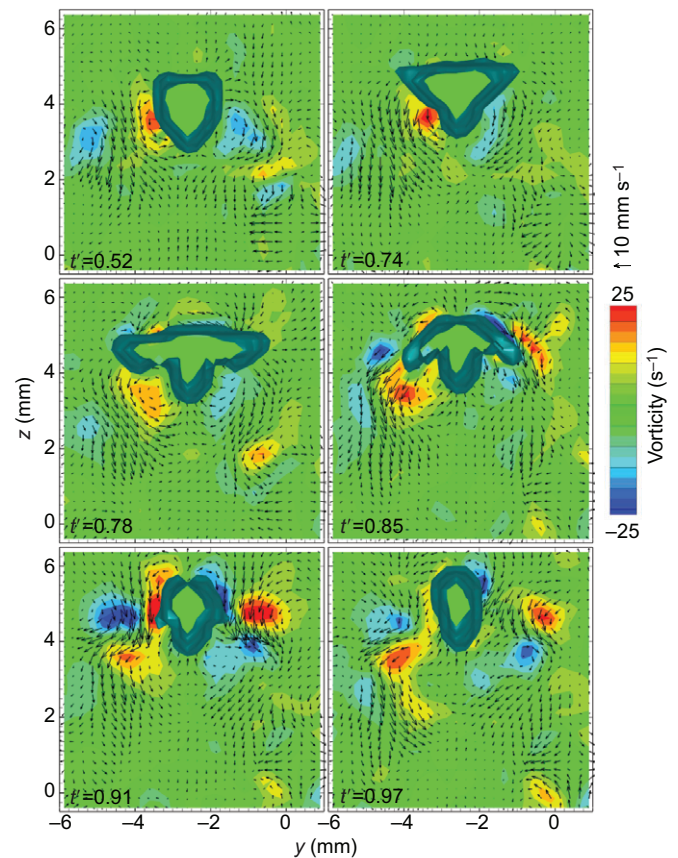

Fig. 9. Flow fields during the recovery stroke. Color contours represent the *x*-component of vorticity. Vectors, which lie tangent in the plane, indicate flow direction and magnitude. The transverse plane, which bisects the shell at mid-recovery stroke, is 0.8 mm more anterior than that shown in Figs 6 and 8.

Power stroke

Separation of the parapodia at the beginning of the power stroke draws fluid downward into the growing, V-shaped gap between the wings ($t'=0.18$–0.22 in Fig. 6). The time variation of the angle α between the wings during the fling is shown in Fig. 7. As the parapodia separate anteriorly to posteriorly, the downward flow also has an out-of-plane component. By $t'=0.24$, the flow has separated from both wingtips to form elongated leading edge vortices, a process that continues at $t'=0.27$. By $t'=0.32$ (Fig. 8), these vortices have strengthened and are in the process of being shed from the wingtips. Shear layers at the base of each wing also begin to develop as the pteropod rises through the leading edge vortices, pushing a bow wave upward in front of the pteropod's shell. This upwards flow is pushed down along the pteropod's wings by the now-shed leading edge vortices, creating an elongated region of high vorticity along each wing ($t'=0.35$–0.37). At $t'=0.37$, the parapodia are approaching the sides of the shell, and flow on the wing upper surface continues to follow the wing down, at speeds up to approximately 13 mm s^{-1}. Maximum flow speeds reach 20 mm s^{-1} at $t'=0.42$ as the parapodia close along the sides of the shell, and this flow continues to feed the leading edge vortex rings. The downward impulse of flow created by the power stroke is evident at $t'=0.48$ (on both sides of the pteropod). A new pair of oppositely signed vortices beneath the pteropod is created by the interaction of these downward pulses and the flow pulled upward beneath the pteropod shell. By $t'=0.52$, the vortices, moving downward and away from the pteropod at an angle of approximately 45 deg relative to vertical, have separated from the shell and begun to decay.

Recovery stroke

Flow fields detailing the recovery stroke are shown in Fig. 9. The t'=0.52 time point is shown in both Figs 8 and 9 in order to illustrate the three-dimensional nature of the flow. In the posterior plane (Fig. 8), the downward flow pulse created at the end of the power stroke moves outward away from the pteropod. In Fig. 9, the downward flow pulse moves more vertically downward and curves back up underneath the pteropod, likely because the parapodia complete the power stroke by curling upward along the shell. The shed leading edge vortices also are weaker and lower in the more anterior plane. In addition, the vorticity patches bound to the pteropod body in the anterior plane (Fig. 9) are not present in the posterior plane (Fig. 8). At t'=0.74, the downward flow along the sides of the pteropod resulting from the power stroke remains (and persists throughout the recovery stroke). The parapodia are well into the recovery stroke, and vorticity has formed on the parapodia's upper leading edges. These vortices grow slightly but remain attached to the wings at t'=0.78. By t'=0.85, these leading edge vortices have strengthened and separated from the parapodia. Downward flow from the wingtips joins with the downward flow created by the power stroke to strengthen the pre-existing vortices underneath the parapodia. Similar to the power stroke, the rising pteropod pushes a bow wave ahead, which curves around and downward to create an elongated high vorticity region along the parapodia, a trend that continues at t'=0.91. Also at t'=0.91, the shed leading edge vortex is strengthened by the downward impulse from the recovery stroke. These vortices subsequently decay and translate away from the pteropod, as seen at t'=0.97, until, at the beginning of the next power stroke, they resemble those vortices seen at t'=0.06 in Fig. 6.

DISCUSSION

Hyper-pitching

Limacina helicina generates its figure-of-eight wingtip trajectory in a unique manner that has implications for micro aerial vehicle (MAV) design. Figure-of-eight wingtip trajectories seen in flying insects (Weis-Fogh, 1973) and shell-less gymnosomatous pteropods (Satterlie et al., 1985; Borrell et al., 2005; Szymik and Satterlie, 2011) are accomplished by active elevation of the wingtip in preparation for the next half-stroke. In *L. helicina*, the figure-of-eight pattern is enabled by extreme rotation of the shell. This hyper-pitching of 50–60 deg elevates the wingtips at the end of each half-stroke in preparation for the next half-stroke and accounts for 25% and 51% of wing elevation at the beginning of the recovery and power strokes, respectively. *Limacina helicina*'s round shell, with a low moment of inertia and low rotational drag, naturally facilitates this hyper-pitching whereas the elongated bodies of the gymnosomatous pteropods have a greater moment of inertia and greater rotational drag and thus experience correspondingly less body rotation (11 deg in *Clione antarctica*) (Borrell et al., 2005). Such extreme pitching during regular swimming or flying is rare, although Kiørboe et al. (2010) found body pitching up to 55 deg in a jumping *Acartia tonsa* copepod. Many insects fly with body angle oscillations of 3 deg or less (Ellington, 1984a). Body kinematics are difficult to measure in the tiny insects flying in the same *Re* range as *L. helicina*, but high-speed videos show little variation in body angle with individual wingbeats for thrips (Santhanakrishnan et al., 2014). In contrast, Dudley (1990) found a much larger range for butterflies, with some species attaining body angle oscillations of 49 deg. Indeed, Chang and Yen (2012) compared the erratic flight of butterflies with the swimming of *L. helicina* and suggested that, like butterflies, pteropods may evade predators with their irregular trajectories brought on by hyper-pitching. While pitching is typically avoided in

flapping MAV design and typical insect flight because of the problems it poses for vehicle or animal stability and control, *L. helicina* 'flight' suggests the opposite paradigm and that hyper-pitching could be incorporated into future MAV designs to passively provide aerodynamic benefits. However, difficulties in maintaining control and stability and in gathering and integrating sensory information while hyper-pitching need to be investigated further.

Flexible clap-and-fling: lift augmentation by the Weis-Fogh mechanism

Similar to many small insect species, *L. helicina* uses a version of the Weis-Fogh clap-and-fling mechanism to generate lift during its power stroke (Fig. 6). The flow generated by the Weis-Fogh mechanism has not previously been measured in a freely flying or swimming animal despite being extensively studied for 40 years (Weis-Fogh, 1973; Lighthill, 1973; Maxworthy, 1979; Ellington, 1984a,b; Spedding and Maxworthy, 1986; Dickinson et al., 1999; Miller and Peskin, 2005; Lehmann et al., 2005; Kolomenskiy et al., 2011). In the classic Weis-Fogh mechanism, the wings clap together at the end of the recovery stroke and subsequently rotate apart in the power stroke, with the trailing edge serving as a 'hinge'. The growing, V-shaped gap draws in fluid, initiating leading edge vortices around each wing, thereby increasing circulation around both wings and increasing lift (Weis-Fogh, 1973; Lighthill, 1973; Maxworthy, 1979; Ellington, 1984a,b; Spedding and Maxworthy, 1986; Dickinson et al., 1999). As the pteropod's wings only touch at their tips and do not fully clap together at the end of the recovery stroke, however, the pteropod's wing motions are better characterized as a 'near-fling' or 'touch-and-fling' rather than a clap-and-fling.

The flow fields captured here, with elongated leading edge vortices forming and eventually shedding, show qualitative agreement with dynamically scaled laboratory experiments and with simulations of insect flight at similar *Re* (Maxworthy, 1979; Spedding and Maxworthy, 1986; Miller and Peskin, 2005; Lehmann et al., 2005; Kolomenskiy et al., 2011). However, the spatial extent of the leading edge vortices relative to the wing size appears larger in the dynamically scaled experiments than in the current study (see Maxworthy, 1979). This observation may have important ecological consequences, as minimizing a 'hydrodynamic footprint' while swimming is an important strategy for zooplankton to avoid predators, which often detect their prey through flow disturbances (Yen, 2000; Kiørboe et al., 2014). The distance between the wings at the beginning of the power stroke may affect the scale of these vortices and the lift augmentation from the Weis-Fogh mechanism.

A mid-span gap between the parapodia at the beginning of the power stroke likely decreases lift augmentation from the Weis-Fogh mechanism. This mid-span gap of approximately the shell width (~1 mm) results from lateral separation of the thick, fleshy wing bases and from wing curvature during the stroke. The center-to-center gap between the parapodia at their insertion point is approximately 0.3 mm, and the wing thickness at the insertion point is approximately 0.2 mm. The gap width decreases towards the wingtips as the highly flexible parapodia curve inwards to meet at their tips. Thus, in contrast to many insect species, the wings of *L. helicina* do not lie parallel along their span at the beginning of the fling (Chang and Yen, 2012). Lehmann et al. (2005) investigated the importance of this gap between the wings in a dynamically scaled model of a fruit fly by varying the lateral separation between the wing hinges and the angular distance between the wings at the beginning of the fling phase (α in this study). These authors found that

Table 2. Comparison of morphological and swimming characteristics of various swimming pteropod species

Species	Reference	Animal length (mm)	Wing length (mm)	Wing chord (mm)	Swimming speed (mm s^{-1})	Wingbeat frequency (Hz)	Re_c	Upstroke angle of attack (deg)	Downstroke angle of attack (deg)	Stroke plane angle (deg)	Sinking speed (mm s^{-1})
Clione limacina	Satterlie et al. (1985)	Up to 20	Can exceed 5	4.5	100	1–3	Estimated at 200	NA	NA	15–20	7–10
	Syzmik and Satterlie (2011)	3–7	3.4–7.7	3.3–7.8	Tethered	1.1–3.2	48–319	59–63	64–70	12–17	NA
Clione antarctica	Borrell et al. (2005)	7–22	2.4–4.5	1.8–5.4	1–7	0.8–1.6	15–123	63–80	NA	19–32	NA
Limacina helicina	Chang and Yen (2012)	1–3.4	1–4	Variable	13–44	4.5–9.4	NA	NA	NA	NA	5–45
	Current study	1.6–2	2.1–2.9	0.5–0.6	15–26	4.3–4.7	49–60	49	46	29	NA

NA, not available.

increasing both of these parameters decreased the lift augmentation due to clap-and-fling. Specifically, for minimum lateral separation and initially parallel wings (α=0 deg), lift was enhanced 13.3% compared with a case with only one wing (i.e. no interaction between wings), whereas it was enhanced only about 4% for a greater lateral separation for the same initial α. In the case of *L. helicina*, wing separation likely also decreases the lift generated by clap-and-fling by allowing inward flow from the wing edges, thereby decreasing the strength and size of the leading edge vortices at the wingtips. However, the lateral wing separation of *L. helicina* allows the touching wings to angle inward and form a 'canopy' over its body. In Lehmann et al. (2005), this canopy effect (called a 'negative angular distance') is modeled for the greater lateral separation and led to a further increase in clap-and-fling lift augmentation to 9% (again compared with a one-wing case). Thus, though the gap between the wings of *L. helicina* seems to decrease the hydrodynamic benefit of the Weis-Fogh mechanism, this may be somewhat offset because of the canopy effect. It should be noted that the canopy effect is not represented in Fig. 7 (i.e. the minimum value of α is 0 deg) as only one point between the parapodia bases (point A) was tracked.

The act of flinging apart closely apposed wings generates both high lift and high drag forces. Using a 2D computational model, Miller and Peskin (2005) found substantial drag forces involved in rotating closely apposed wings apart during the fling. In addition, Santhanakrishnan et al. (2014) varied the initial gap between porous wings and found large increases in drag and only modest increases in lift with more closely spaced wings. Thus, while the mid-span gap between the wings of *L. helicina* at the beginning of the fling likely decreases lift, this gap also likely reduces drag on the wings during the fling, thus lowering the force requirements on the animal. Furthermore, Miller and Peskin (2009) found that adding flexibility to the wing reduced the drag forces while maintaining lift forces during the fling. Jones et al. (2015) similarly found that wing flexibility increased vertical force production in a simulated, tilted wing stroke similar to that used by *L. helicina*. Thus, the highly flexible parapodia of *L. helicina* also may reduce drag while sustaining lift during the fling and throughout the stroke.

It is difficult to estimate the relative importance of the Weis-Fogh mechanism in enhancing lift for *L. helicina*. Lehmann et al. (2005) measured lift enhancements of up to 17% for their dynamically scaled *Drosophila* model, but this augmentation depended greatly on lateral and angular wing separation and other kinematic parameters (Lehmann and Pick, 2007). Lift augmentation by the Weis-Fogh mechanism is also dependent on Reynolds number. The computational model of Miller and Peskin (2005) shows increased lift enhancement with decreasing *Re*, whereas the experimental results of Lehmann et al. (2005) do not show a clear trend. *Limacina helicina* operates at a lower *Re* than *Drosophila*, but *L. helicina* may also use other unsteady flow techniques to increase lift production. For example, Chang and Yen (2012) suggested that the clap of the parapodia against the shell at the end of the power stroke could create thrust by squeezing fluid downwards. Another possibility is that the parapodia peeling away from the shell at the beginning of the recovery stroke may generate lift. Occlusion by the shell and parapodia make it difficult to determine whether these mechanisms are present in the current case.

Comparison with other planktonic gastropods

It is interesting to compare *L. helicina* swimming with that of the shell-less pteropods *Clione limacina* and *C. antarctica*. As seen in Table 2, the shell sizes of *L. helicina* in the current study are substantially smaller than the body lengths of the gymnosomatous pteropods. The swimming speeds of *L. helicina* are slower than those of its predator *C. limacina* but faster than those of *C. antarctica*. Accounting for body size, however, shows that *L. helicina*, *C. limacina* and *C. antarctica* swim at maximum normalized swimming speeds of approximately 13, 5 and 0.3 body lengths s^{-1}, respectively. The slower swimming speeds of *C. antarctica* perhaps may be partially explained by the higher viscosity of the cold, polar seawater. The wingbeat frequency of *L. helicina* is also higher than those of the shell-less pteropods. The faster normalized swimming speed and greater beat frequency of *L. helicina* indicate that it is a more agile swimmer than its predator, the shell-less *C. limacina*. The high beat frequency of *L. helicina*, coupled with its extreme pitching angle, should enable it to frequently change swimming direction. The resulting tortuous swimming pathway may enable it to evade the larger, more slowly stroking *C. limacina* that depends on tail bending to change swimming direction (Satterlie et al., 1985).

The shell of *L. helicina* also plays a large role in its swimming behavior. In addition to facilitating the hyper-pitching discussed above, the shell's weight obviously leads to a greater sinking speed for *L. helicina* and a greater need for it to generate lift than for the shell-less pteropods. The shell also ensures that the swimming

appendages of *L. helicina* have closely spaced insertion points, a morphological arrangement that allows this pteropod's parapodia to closely approach each other and perform the lift-enhancing Weis-Fogh maneuver. The appendages of the shell-less pteropods, in contrast, are located on opposite sides of its torpedo-shaped body and cannot approach each other along their length. Satterlie et al. (1985) posited that *C. limacina* peels its appendages away from its body in a way that could create lift, but no flow measurements have been performed on *Clione* to investigate its lift generation mechanisms. Whereas we have shown that *L. helicina* mimics the lift-producing kinematics and fluid dynamics of insects, the fluid dynamics of the flow around the wings of the *Clione* species are essentially unknown. The outcomes among studies of *Clione* swimming are contradictory, with Satterlie et al. (1985) concluding that the wing movement of *C. limacina* produces lift in both upstroke and downstroke, Borrell et al. (2005) concluding that pteropods are poorly equipped to propel via lift forces, and Szymik and Satterlie (2011) concluding that *C. limacina* propulsion is provided by a combination of lift-based and drag-based mechanisms. Flow measurements would be valuable in resolving this uncertainty.

CONCLUSIONS

Our measurements strongly indicate that *L. helicina* uniquely employs lift-based swimming instead of drag-based swimming used by nearly all zooplankton. This pteropod 'flies' underwater by stroking its parapodia in a figure-of-eight trajectory at a high angle of attack with an inclined stroke plane in much the same way that tiny insects such as thrips and fruit flies fly in air. The wing kinematic pattern is uniquely facilitated by *L. helicina*'s hyper-pitching, which also may aid in evasion of predators. Moreover, hyper-pitching offers an alternative vision for flapping MAV design. In accordance with most flying animals, pitching traditionally has been eschewed in favor of body stability, but *L. helicina* demonstrates that extreme pitching, when integrated with wing kinematics, may offer passive aerodynamic benefits. *Limacina helicina* further earns its common name of 'sea butterfly' by borrowing the Weis-Fogh mechanism from the insect world as it performs a 'near-fling' maneuver to augment lift generation during its power stroke. Though Gastropoda and Insecta diverged 550 million years ago, *L. helicina* and flying insects swim and fly, respectively, in similar physical environments (at least in terms of the balance of inertial and viscous forces as quantified by *Re*) and employ similar wing kinematics and fluid dynamic lift generation mechanisms. *Limacina helicina* and tiny insects thus represent a remarkable evolutionary convergence of locomotion techniques employed by dissimilar animals that operate in a similar *Re* regime. *Clione* species and other planktonic gastropods, which, like *L. helicina*, are also fragile and difficult to study, may also use lift-based locomotion and ought to be further investigated.

Competing interests
The authors declare no competing or financial interests.

Author contributions
J.Y. secured and cared for the pteropods. J.Y., D.W.M. and D.R.W. designed the study. J.Y. and D.W.M. performed the experiments. D.W.M. and D.A. processed the tomographic PIV data for flow fields and kinematics. D.W.M., D.R.W., D.A. and J.Y. wrote the manuscript. All authors approved the final manuscript.

Supplementary information
Supplementary information available online at
http://jeb.biologists.org/lookup/suppl/doi:10.1242/jeb.129205/-/DC1

References

Adhikari, D. and Longmire, E. K. (2012). Visual hull method for tomographic PIV measurement of flow around moving objects. *Exp. Fluids* **53**, 943-964.

Bednaršek, N., Tarling, G. A., Fielding, S. and Bakker, D. C. E. (2012). Population dynamics and biogeochemical significance of *Limacina helicina antarctica* in the Scotia Sea (Southern Ocean). *Deep Sea Res. II Top Stud Oceanogr* **59-60**, 105-116.

Borrell, B. J., Goldbogen, J. A. and Dudley, R. (2005). Aquatic wing flapping at low Reynolds numbers: swimming kinematics of the Antarctic pteropod, *Clione antarctica*. *J. Exp. Biol.* **208**, 2939-2949.

Chang, Y. and Yen, J. (2012). Swimming in the intermediate Reynolds range: kinematics of the pteropod *Limacina helicina*. *Integr. Comp. Biol.* **52**, 597-615.

Cooter, R. J. and Baker, P. S. (1977). Weis-Fogh clap and fling mechanism in *Locusta*. *Nature* **269**, 53-54.

Dickinson, M. H. and Götz, K. G. (1996). The wake dynamics and flight forces of the fruit fly *Drosophila melanogaster*. *J. Exp. Biol.* **199**, 2085-2104.

Dickinson, M. H., Lehmann, F.-O. and Sane, S. P. (1999). Wing rotation and the aerodynamic basis of insect flight. *Science* **284**, 1954-1960.

Dudley, R. (1990). Biomechanics of flight in neotropical butterflies: morphometrics and kinematics. *J. Exp. Biol.* **150**, 37-53.

Ellington, C. P. (1984a). The aerodynamics of hovering insect flight. III. Kinematics. *Philos. Trans. R. Soc. B Biol. Sci.* **305**, 41-78.

Ellington, C. P. (1984b). The aerodynamics of hovering insect flight. IV. Aerodynamic mechanisms. *Philos. Trans. R. Soc. B Biol. Sci.* **305**, 79-113.

Fuchiwaki, M., Kuroki, T., Tanaka, K. and Tababa, T. (2013). Dynamic behavior of the vortex ring formed on a butterfly wing. *Exp. Fluids* **54**, 1450.

Gilmer, R. W. and Harbison, G. R. (1986). Morphology and field behavior of pteropod molluscs: feeding methods in the families Cavoliniidae, Limacinidae and Peraclididae (Gastropoda: Thecosomata). *Mar. Biol.* **91**, 47-57.

Hays, G. C. (2003). A review of the adaptive significance and ecosystem consequences of zooplankton diel vertical migrations. In *Migrations and Dispersal of Marine Organisms* (ed. M. B. Jones, A. Ingólfsson, E. Ólafsson, G. V. Helgason, K. Gunnarsson and J. Svavarsson), pp. 163-170. The Netherlands: Kluwer Academic Publishers.

Hedrick, T. L. (2008). Software techniques for two- and three-dimensional kinematic measurements of biological and biomimetic systems. *Bioinspir. Biomim.* **3**, 034001.

Jones, S. K., Laurenza, R., Hedrick, T. L., Griffith, B. E. and Miller, L. A. (2015). Lift vs. drag based mechanisms for vertical force production in the smallest flying insects. *J. Theor. Biol.* **384**, 105-120.

Kiørboe, T., Andersen, A., Langlois, V. J. and Jakobsen, H. H. (2010). Unsteady motion: Escape jumps in planktonic copepods, their kinematics and energetics. *J. R. Soc. Interface* **7**, 1591-1602.

Kiørboe, T., Jiang, H., Gonçalves, R. J., Nielsen, L. T. and Wadhwa, N. (2014). Flow disturbances generated by feeding and swimming zooplankton. *Proc. Natl. Acad. Sci. USA* **111**, 11738-11743.

Kolomenskiy, D., Moffatt, H. K., Farge, M. and Schneider, K. (2011). The Lighthill–Weis-Fogh clap–fling–sweep mechanism revisited. *J. Fluid Mech.* **676**, 572-606.

Lehmann, F.-O. and Pick, S. (2007). The aerodynamic benefit of wing-wing interaction depends on stroke trajectory in flapping insect wings. *J. Exp. Biol.* **210**, 1362-1377.

Lehmann, F.-O., Sane, S. and Dickinson, M. (2005). The aerodynamic effects of wing-wing interaction in flapping insect wings. *J. Exp. Biol.* **208**, 3075-3092.

Lighthill, M. J. (1973). On the Weis-Fogh mechanism of lift generation. *J. Fluid Mech.* **60**, 1-17.

Maxworthy, T. (1979). Experiments on the Weis-Fogh mechanism of lift generation by insects in hovering flight. Part 1. Dynamics of the 'fling'. *J. Fluid Mech.* **93**, 47-63.

McGhee, G. (2011). *Convergent Evolution*. Cambridge, MA: MIT Press.

Miller, L. A. and Peskin, C. S. (2005). A computational fluid dynamics of 'clap and fling' in the smallest insects. *J. Exp. Biol.* **208**, 195-212.

Miller, L. A. and Peskin, C. S. (2009). Flexible clap and fling in tiny insect flight. *J. Exp. Biol.* **212**, 3076-3090.

Murphy, D. W., Webster, D. R. and Yen, J. (2012). A high-speed tomographic PIV system for measuring zooplanktonic flow. *Limnol. Oceanogr. Methods* **10**, 1096-1112.

Murphy, D. W., Webster, D. R. and Yen, J. (2013). The hydrodynamics of hovering in Antarctic krill. *Limnol. Oceanogr. Fluids Environ.* **3**, 240-255.

Santhanakrishnan, A., Robinson, A. K., Jones, S., Low, A. A., Gadi, S., Hedrick, T. L. and Miller, L. A. (2014). Clap and fling mechanism with interacting porous wings in tiny insect flight. *J. Exp. Biol.* **217**, 3898-3909.

Satterlie, R. A., LaBarbera, M. and Spencer, A. N. (1985). Swimming in the pteropod mollusk *Clione limacina*. 1. Behaviour and morphology. *J. Exp. Biol.* **116**, 189-204.

Spedding, G. R. and Maxworthy, T. (1986). The generation of circulation and lift in a rigid two-dimensional fling. *J. Fluid Mech.* **165**, 247-272.

Strickler, R. (1975). Swimming of planktonic Cyclops species (Copepoda, Crustacea): pattern, movements and their control. In *Swimming and Flying in Nature*, Vol. 2. (ed. T. Wu, C. Brokaw and C. Brennen), pp. 599-613. New York: Plenum Press.

Szymik, B. G. and Satterlie, R. A. (2011). Changes in wingstroke kinematics associated with a change in swimming speed in a pteropod mollusk, Clione limacina. *J. Exp. Biol.* **214**, 3935-3947.

Valentine, J. W. (1997). Cleavage patterns and the topology of the metazoan tree of life. *Proc. Natl. Acad. Sci. USA* **94**, 8001-8005.

Vogel, S. (1967). Flight in Drosophila II: variations in stroke parameters and wing contour. *J. Exp. Biol.* **46**, 383-392.

Walker, J. A. and Westneat, M. W. (2000). Mechanical performance of aquatic rowing and flying. *Proc. R. Soc. B Biol. Sci.*. **267**, 1875-1881.

Wang, Z. J. (2004). The role of drag in insect hovering. *J. Exp. Biol.* **207**, 4147-4155.

Weis-Fogh, T. (1973). Quick estimates of flight fitness in hovering animals, including novel mechanisms for lift production. *J. Exp. Biol.* **59**, 169-230.

Weis-Fogh, T. (1975). Unusual mechanisms for the generation of lift in flying animals. *Sci. Am.* **233**, 80-87.

Yen, J. (2000). Life in transition: balancing inertial and viscous forces by planktonic copepods. *Biol. Bull.* **198**, 213-224.